 doi:10.20944/preprints201910.0133.v1

Article

Experimental Study of the Performance of A Novel Vertical Axis Wind Turbine

J. Agbormbai[1] and W.D. Zhu[2]

[1]University of Maryland, Baltimore County,1000 Hilltop Circle, Baltimore, MD 21250;USA; jagborm1@umbc.edu

[2]University of Maryland, Baltimore County,1000 Hilltop Circle, Baltimore, MD 21250; USA; wzhu@umbc.edu

Correspondence: jagborm1@umbc.edu; wzhu@umbc.edu

Abstract: *The basic equation for estimating the aerodynamic power captured by an Anderson Vertical Axis Wind Turbine (AVAWT) is a solution of the Navier-Stokes(N-S) equations for a baroclinic, inviscid flow. In a nutshell, the pressure difference across the AVAWT is derived from Bernoulli's equation; an upshot of the integration of the N-S momentum equation for a baroclinic inviscid flow, Euler's momentum equation. The resulting expression for the pressure difference across the AVAWT rotor is plotted as a function of freestream speed. Experimentally determined airstream speeds at the AVAWT inlet and outlet, coupled with corresponding freestream speeds are used in estimating the aerodynamic power captured. The aerodynamic power is subsequently used in calculating the aerodynamic power coefficient of the AVAWT. The actual power coefficient is calculated from the power generated by the AVAWT at various free stream speeds and plotted as a function of the latter. Experimental results show that, at all free stream speeds and tip speed ratios, the aerodynamic power coefficient is higher than the actual power coefficient of the AVAWT. Consequently, the power generated by the AVAWT prototype is lower than the aerodynamic power captured, given the same inflow wind condition.*

Keywords: Anderson-Vertical-Axis-Wind-Turbine, Actual-Power, Aerodynamic-Power, Blockage-Factor, Power-Coefficient, Tip-speed-Ratio

 doi:10.20944/preprints201910.0133.v1

1. Introduction

Albeit vertical axis wind turbines are not new to subject matter experts, it is worthwhile shedding some light on them so that, readers who are not subject matter experts can acquire some knowledge about these contrivances. Besides the VAWT under investigation is a new contraption, something which makes an overview of existing VAWTs relevant. In their bid to demonstrate the aerodynamic feasibility of a curved bladed Darrieus vertical axis wind turbine (VAWT) rotor, engineers at the Sandia Laboratory of the US department of energy (USDOE) developed a 5m diameter two bladed prototype which was mounted on the roof of their laboratory and observed to rotate on windy days. Following the afore-mentioned rotor was the development of a 17m diameter curved, two bladed rotor which was observed to perform nearly as efficiently as a horizontal axis wind turbine (HAWT) rotor of equal capacity. A 34m diameter VAWT of same type, called the test rig by Sandia, was developed thereafter and incorporated with instruments for condition monitoring and instruments to record weather conditions that affect its performance. Sandia laboratory also uses this VAWT to; validate various computer models, test airfoil designs and develop various control strategies [1]. Unlike this study that performs a wind tunnel experiment to investigate the performance of a novel VAWT, the Sandia laboratory performs on-site investigations on a working VAWT.

Typically, VAWTs may have either drag-driven or lift-driven rotors. The Savonius rotor is the most common drag driven rotor. It has been used on water pumps and is cheap to manufacture. Savonius machines typically have low power coefficients because of their being drag driven. Power coefficients of about 0.30 are typical of Savonius rotors. Additionally, they have solidity close to unity, so-much-so that, they are very heavy relative to their power production capacity and it is also difficult to protect them from high winds [2].

The Darrieus VAWT is a lift-driven machine. Lift-Driven VAWTs have almost always been used for electrical power generation. Lift-driven VAWTs typically have rotors with straight blades or curved blades. Some VAWTs with straight blade rotors have a pitching mechanism, even though most lift driven VAWTs have fixed blades. Yawing mechanisms are not needed on VAWTs, since they see the wind in any direction. The rotor blades of lift driven VAWTs are generally untwisted and are of constant chord, thus, they are easy to mass-produce. VAWTs are prone to high fatigue damage because, the load on each blade varies during each rotation of the rotor. They are difficult to support on separate tall towers, since a large portion of the rotor tends to be close to the ground in a region of low wind speed. This results in less productivity, compared to a HAWT of the same capacity [2,3].

In 1988, a 100m high, 60m diameter Darrieus VAWT was installed in Canada. The 60m diameter VAWT ran for six years with 94% availability [2]. As stated earlier on, Darrieus VAWTs work on the principle of aerodynamic lift (i.e. the wind pulls the rotor blades along). On the contrary the traditional Holland type windmill operates on the principle of drag (i.e. the wind pushes a manmade barrier such as a rotor blade) [1]. Typically, Darrieus VAWTs have power coefficients between 0.4 and 0.42 [4]. They are not self-starting; some drag ought to be imposed on them for them to be able to be self-starting. The installation of cups or vanes on Darrieus VAWTs, makes them capable of trapping the wind, thus causing them to self-start [1,3]. Using the foregoing methods to self-start the Darrieus VAWT, results in larger blades, such that, these methods were abandoned.

To encourage the development of wind energy technology in the United States, the Federal Government gave incentives such as a tax credit of 1.80cents/KWh of wind energy produced. The USDOE set a goal in 2008, to achieve a 20% contribution to grid power by wind energy sources by the year 2030 [1]. This is clear evidence of the fact that, there is a niche for wind energy in the US energy market.

 doi:10.20944/preprints201910.0133.v1

VAWTs can effectively be used in urban areas where turbulent and unsteady wind is typical [5,6]. They have inherent superiority over HAWTs in severe wind conditions, because, the wind enters their rotors from about any direction without yawing. A discrepancy factor of 2 typically exists between computational fluid dynamics (CFD) and wind tunnel experiment results; since, the effect of finite blade length and spoke drag are not usually considered in CFD analysis. The performance of a VAWT with a steady inflow condition is not a reflection of the actual performance of a VAWT operating in an urban environment, an upshot of the fact that, the wind fluctuates in an urban environment. The wind turbine's performance depends on the cube of the speed of the inflow wind, thus, moderate fluctuations in wind speed would result in very large fluctuations in power [5]. The seeming stagnation in improvements on the aerodynamics of HAWTs has spurred up interest in the development of large scale VAWTs. Another factor in favor of VAWTs is the future demand for decentralized and sustainable energy supply in Cities and rural communities [7]. They are suitable where HAWTs do not operate efficiently, usually in locations with high wind speeds and turbulent wind flow. VAWTs are quieter than HAWTs, something which makes them suitable for use in urban areas [8,9].

Savonius VAWTs can withstand gusts because of their superior stalling behavior and are suitable for use in gusty environments. At a tip speed ratio of unity, the power coefficient of a Savonius rotor is maximum. Modifications on the blade geometry of Savonius rotors improve the power coefficient. The power coefficient of a Savonius rotor with a 45º angle of twist is 0.3385 compared to the 0.30 for rotors with untwisted blades. Two stage Savonius rotors perform better than their three stage counterparts. Both three bladed and two bladed Savonius rotors exhibit high power coefficients at low tip speed ratios [8].

Curved Darrieus VAWTs with troposkein shapes are prone to nearly tensile loads and minimal bending moments on the rotor blades. They operate at distinct angles of attack at different azimuth angles and are subjected to cyclic aerodynamic loads which can result in fatigue [9]. Cognizant of the afore-mentioned setback on the curved Darrieus VAWTs and other VAWTs, the conduction of experiments and simulations in order to ascertain their suitability for use is imperative. The International Electro-Technical Commission (IEC) guidelines include well established procedures for wind turbine testing. Based on IEC guidelines, the service life of Wind Turbines (WT) is 20 years. Breakdown times are frequent with WTs and such breakdown stem from manufacturing errors and design errors due to underestimated fatigue load or extreme loads. Consideration of turbulent inflow conditions during aerodynamic modelling is of paramount importance. The turbulent characteristics of the inflow air may have an impact on the fatigue loads experienced by the WT [10].

Blade pitching is more difficult for VAWTs than for HAWTs because of the dependence of the angle of attack of the former on the rotor azimuth angle; resulting in the existence of very few practical pitch control schemes for VAWTs [11]. Unlike some of the existing VAWTs which may require pitch control to maximize wind energy capture, the VAWT in this study does not require pitch control for wind energy capture optimization.

The extraction of the wind's momentum by the VAWT occurs more during the upwind pass. Most of the VAWT's power output is produced on the upwind pass whereas flow momentum is considerably reduced on the downwind pass, hence resulting in a reduced power output [12]. Darrieus type VAWTs with straight blades are less efficient than those with helically twisted blades [13].

Various numerical and analytical schemes have been implemented in a bid to investigating the performance characteristics of VAWTs. Zanon et al [14] solved potential flow equations in conjunction with integral boundary layer equations formulated for the VAWT rotor, using a semi-inverse iterative algorithm. From their simulations they inferred that, VAWTs can be designed to avoid the occurrence of dynamic stall resulting from blade-vortex interaction in the downward part of rotor rotation during gusts, normal operation and even at low tip speed ratios [14].Scheurich and others [13] implemented a Computational Fluid Dynamics (CFD) scheme

Preprints (www.preprints.org) | NOT PEER-REVIEWED | Posted: 11 October 2019 doi:10.20944/preprints201910.0133.v1

based on the vortex transport model (VTM). The VTM is based on solving the Navier-Stokes(N-S) equations in terms of vorticity and velocity. The governing momentum equation is expressed in terms of vorticity and velocity and is the result of finding the curl of the velocity and pressure-based N-S momentum equation. In their work on the steady state and dynamic simulations of Savonius rotors, Jaohindy et al [15], found out that, the best approximations of the static torque coefficient, the dynamic torque coefficient and the power coefficient were obtained using the shear stress transport (SST)-k-ω rather than k-ε turbulence models. At startup, the dynamic torque coefficient curves of a Savonius rotor oscillate around fixed values in polar coordinates [15].There is a significant difference between the simulated and experimental values of the power coefficient of a Darrieus VAWT at high tip speed ratios even though simulation and experimental power coefficient values follow the same trend as the tip speed ratio varies [16]. The power coefficient of a Darrieus type VAWT peaks at tip speed ratios between 3 and 4 and drops for tip speed ratios greater than 4 for both CFD simulation results and experimental results with values of the former being slightly higher than those of the latter (See figure 18 of reference [17]).

This study uses an experimental approach to investigate the performance of a novel VAWT. Unlike the CFD simulations performed by some of the cited authors, which were based on two or three tip speed ratios, this study investigates the performance characteristics of the novel VAWT over a broad range of tip speed ratios. The VAWT under investigation is a novel VAWT invented and patented by Bruce E. Anderson, under patent number US8790069.

2.0 Basic Equations of Fluid Dynamics

Stating without proof; for baroclinic flows the integral of the Navier-Stokes equation [18,19,20] results in the Bernoulli's equation given by;

$$\frac{1}{2}|\vec{V}|^2 + \int \frac{\partial p}{\rho} + gz = \mathfrak{M}, \qquad (1)$$

For one dimensional (1-D) baroclinic flows, $\vec{V} = U$ and $\int \frac{\partial p}{\rho} = \frac{p}{\rho}$, yielding;

$$\frac{1}{2}U^2 + \frac{p}{\rho} + gz = \mathfrak{M}, \qquad (2)$$

Applying eqn. (2) to stations 0-1 in Fig. 1, we have;

$\frac{1}{2}U_0^2 + \frac{p_0}{\rho} + gz = \frac{1}{2}U_1^2 + \frac{p_1}{\rho} + gz$ which on further simplifying, yields, $\frac{1}{2}U_0^2 + \frac{p_0}{\rho} = \frac{1}{2}U_1^2 + \frac{p_1}{\rho}$ and

$$\frac{p_1}{\rho} - \frac{p_0}{\rho} = \frac{1}{2}U_0^2 - \frac{1}{2}U_1^2, \qquad (3)$$

Applying eqn. (2) to stations 2-3 in fig. 1 below we have; $\frac{1}{2}U_2^2 + \frac{p_2}{\rho} + gz = \frac{1}{2}U_3^2 + \frac{p_0}{\rho} + gz$, which on simplifying further, yields, $\frac{1}{2}U_2^2 + \frac{p_2}{\rho} = \frac{1}{2}U_3^2 + \frac{p_0}{\rho}$ and

Preprints (www.preprints.org) | NOT PEER-REVIEWED | Posted: 11 October 2019 doi:10.20944/preprints201910.0133.v1

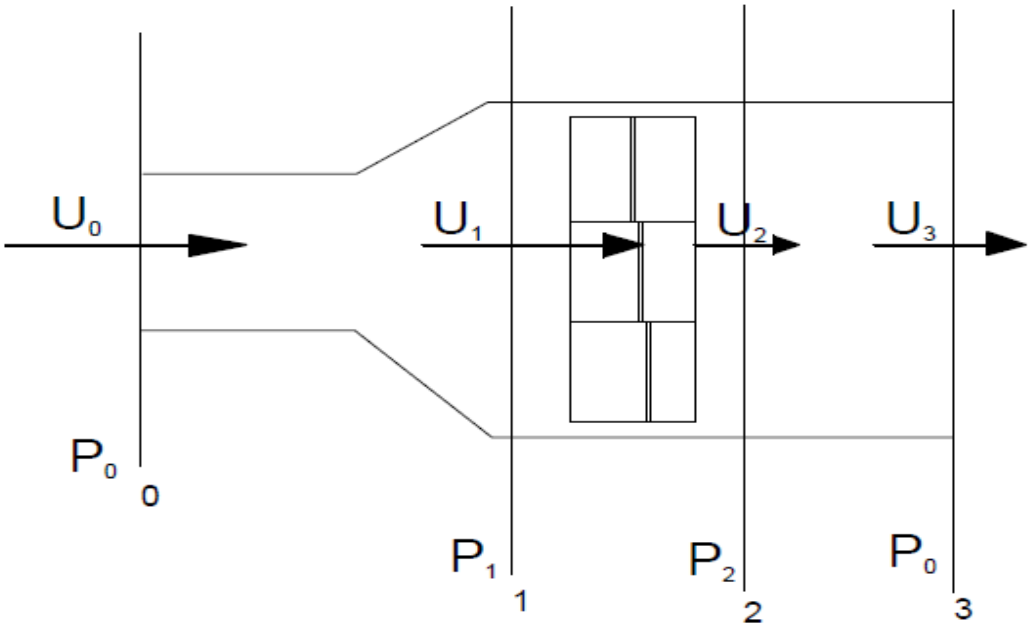

Figure.1 Control Volume of the Anderson VAWT

$$\frac{p_0}{\rho}-\frac{p_2}{\rho}=\frac{1}{2}U_2^2-\frac{1}{2}U_3^2\ , \tag{4}$$

Adding eqn. (3) to eqn. (4) yields;

$$\frac{p_1}{\rho}-\frac{p_2}{\rho}=\frac{1}{2}U_0^2-\frac{1}{2}U_1^2+\frac{1}{2}U_2^2-\frac{1}{2}U_3^2\,. \tag{5}$$

Applying eqn. (2) to stations 1-2 in fig. 1 below we have; $\frac{1}{2}U_1^2+\frac{p_1}{\rho}+gz=\frac{1}{2}U_2^2+\frac{p_2}{\rho}+gz$, which on simplifying further, yields, $\frac{1}{2}U_1^2+\frac{p_1}{\rho}=\frac{1}{2}U_2^2+\frac{p_2}{\rho}$ and

$$\frac{p_1}{\rho}-\frac{p_2}{\rho}=\frac{1}{2}U_2^2-\frac{1}{2}U_1^2, \tag{6}$$

Adding eqns. (5) and (6) yields;

$$2(\frac{p_1}{\rho}-\frac{p_2}{\rho})=\frac{1}{2}U_0^2-U_1^2+U_2^2-\frac{1}{2}U_3^2, \tag{7}$$

Preprints (www.preprints.org) | NOT PEER-REVIEWED | Posted: 11 October 2019 doi:10.20944/preprints201910.0133.v1

Momentum is recovered far downwind the VAWT, because of the atmospheric boundary layer, thus, $U_3 = U_0$ and equation (7) becomes; $\frac{p_1}{\rho} - \frac{p_2}{\rho} = \frac{1}{2}U_2^2 - \frac{1}{2}U_1^2$, which on simplifying further yields the pressure drop across the VAWT below;

$$p_2 - p_1 = \frac{1}{2}\rho(U_1^2 - U_2^2), \quad (8)$$

The wind power captured could be calculated from the rate of change of kinetic energy as follows:

$$Power = \frac{1}{2}\dot{m}(U_0^2 - U_2^2), \quad (9)$$

But $\dot{m} = \rho A U_1$ and equation (9) becomes,

$$Power = \frac{1}{2}\rho A U_1(U_0^2 - U_2^2), \quad (10)$$

The total energy borne by the wind seen by the VAWT is given by,

$$P_{\max} = \frac{1}{2}\rho A U_0^3, \quad (11)$$

The power coefficient, C_p, is given by;

$$C_p = P / P_{\max}, \quad (12)$$

4.0 Aim of the Experiment

The purpose of this experiment is multipronged, namely, to prove that the Anderson Vertical Axis Wind Turbine (AVAT) can generate electricity, to determine the power coefficient of an AVAWT, to investigate its dependence on free stream speed and the tip speed ratio and to investigate the dependence on free stream speed and tip speed ratio of the torque and the power generated.

5.0 Experimental Procedures

The International Electro-Technical Committee's (IEC) standard number: IEC61400-12-1, requires that, on-site measurements of electric power generated by wind turbines be made at respective wind speeds. Based on the afore mentioned, the power generated by the AVAWT model is measured at respective free stream speeds. It is worthwhile noting that, the apparatus used in this experiment consists of a 55.88cm x 60.96cm x182.88cm custom made plywood wind tunnel, a 17.78cm diameter x 41.91cm high AVAWT model, a Benetech hotwire anemometer (Model: GM 8903 with a resolution of $\pm 0.1 m/s$ and a memory of 350 records), a Hylec MS 6252 digital anemometer(with a resolution of $\pm 0.01 m/s$), a Torquesense model RWT421-DD-KG torque transducer with a maximum torque range of 17.5Nm, a steel rule, a try square, a Lenovo Ideapad P400 Touch laptop computer and a Canon PowerShot A570IS digital camera. The torque transducer measures torque, power output and rotational frequency in RPM.

Prior to carrying out the experiment, the setting of the fan used on the wind turbine was calibrated by measuring the speed of air (free stream speed) at the center of the wind tunnel with the AVAWT model not in place, using a hot wire anemometer as shown in plate 1 below. The free stream speed was measured for each of the twelve settings on the fan motor's variable speed drive. All observations were recorded. Experiments were carried out after the necessary safety precautions were followed. All view windows were firmly short, the fan end of the

 doi:10.20944/preprints201910.0133.v1

wind tunnel was provided with a protective wire gauze screen to prevent users from being injured by rotating equipment. Plate 2 and Figure 2 below depict the setup of the experiment.

Plate 1- Setup for the Calibration of the fan setting terms speed (m/s)

Plate 2- Setup for measuring VAWT performance parameters

The AVAWT model was installed in the wind tunnel as shown in plate 2 and Figure 2 and coupled to the torque transducer. The hotwire anemometer was placed at a distance one rotor diameter upstream the AVAWT strategically located to measure the wind speed at the center of the wind tunnel while the digital anemometer was placed two rotor diameters downstream the AVAWT. All leads from measuring instruments to the laptop were connected and the setup was put on by selecting the fan speed and turning on the fan motor. All readings were taken and tabulated.

Preprints (www.preprints.org) | NOT PEER-REVIEWED | Posted: 11 October 2019 doi:10.20944/preprints201910.0133.v1

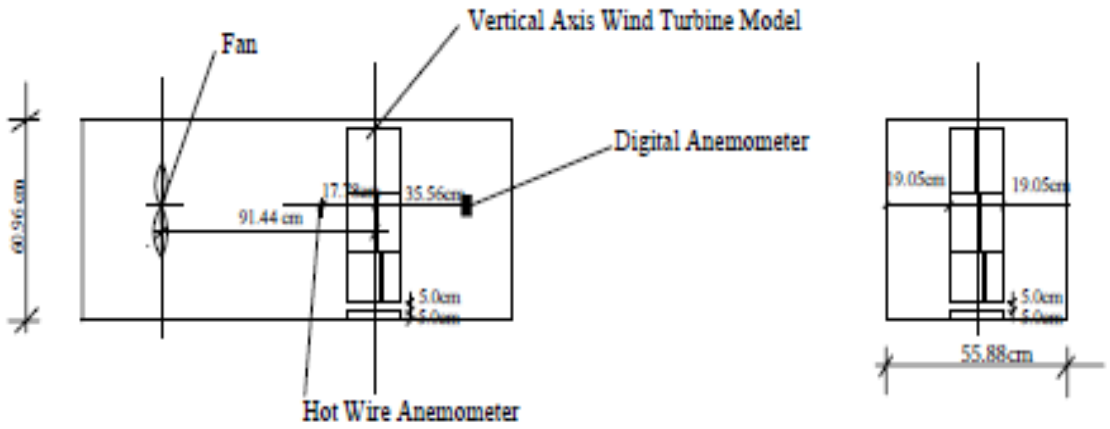

Figure 2- Experimental Setup showing Measurements.

5.1 Observations

It is worth noting that, the fan used in this experiment has 12 speed settings; seven of the speed setting lie between 1.77m/s and 3.3m/s. These speed settings imparted no rotation on the AVAWT, so their results were discarded. The recorded measurements of respective parameters at respective free stream speeds are shown in table 1 below. Table 4 contains the estimated induction factors at the AVAWT inlet and outlet respectively.

5.2 Precision

Torque transducer measurements are within a margin of accuracy of $\pm 0.25\%$. The hotwire anemometer measurements are within a margin of accuracy of $\pm 3.0\%$, while the digital anemometer readings are within a margin of accuracy of $\pm 2.0\%$.

5.3 Calculations

The angular speed of the AVAWT is calculated from the measured RPM using eqn. (13) below:

$$\omega = \frac{2\pi RPM}{60}, \qquad (13)$$

The rotational power is calculated from the angular speed and the measured torque, T, as follows;

$$P_{rot} = T\omega, \qquad (14)$$

P_{actual}, the average power is reckoned from the measured electrical power and the rotational power using eqn. (15) below;

$$P_{actual} = \frac{P_{rot} + P}{2}, \qquad (15)$$

P_{aero}, the aerodynamic power is given by eqn. (10) above as follows;

$$P_{aero} = \frac{1}{2}\sigma A U_1 (U_0^2 - U_2^2), \qquad (16)$$

Preprints (www.preprints.org) | NOT PEER-REVIEWED | Posted: 11 October 2019 doi:10.20944/preprints201910.0133.v1

The respective power coefficients are estimated from eqn. (17) as follows:

$$C_{p,actaul} = P_{actual} / P_{\max}, \quad (17a)$$

$$C_{p,aero} = P_{aero} / P_{\max}, \quad (17b)$$

The tip speed ratio is given by eqn. (18) below;

$$\lambda = \frac{\omega R}{U_0}, \quad (18)$$

Where R is the radius of the AVAWT rotor. The induction factor at the AVAWT inlet, a is given by;

$$a = \frac{U_0 - U_1}{U_0}, \quad (19a)$$

The average induction factor $\bar{a}$ is given by;

$$\bar{a} = (1/5)\sum a, \quad (19b)$$

The multiplication factor on the induction factor at the AVAWT exit, m is given by;

$$m = \frac{U_0 - U_2}{aU_0}, \quad (20a)$$

$$\bar{m} = (1/5)\sum m, \quad (20b)$$

6.0 Results and Discussion

Experimental data are used to estimate the parameters expressed in eqns. (8) through (20b) and tabulated as shown in tables 2, 3 and 4 below. Figures 3 to 10 below depict graphs plotted from experimental results. The average induction factor, $\bar{a}$, calculated from experimental measurements of the upwind and downwind free stream speeds using Eqns. (19a and b) is 0.642 ± 0.876 and the downwind speed could be expressed as $U_2 = U_0(1 - \bar{m}a)$. Where $\bar{m}$ is an average value estimated from measured upwind and downwind speeds using Eqns. (20a and b) and is 1.34 ± 0.1122. Thus, the AVAWT rotor inlet and outlet air speeds are given as follows;

U_0 (m/s)	**Power Output(W)**	**Torque (Nm)**	**RPM**
4.22±0.1300	0.60±0.0020	0.046±0.0001	105±0.2620
7.65±0.2300	1.42±0.0040	0.052±0.0001	270±0.6750
9.39±0.2820	8.63±0.220	0.161±0.0004	578±1.4500
9.65±0.2890	9.94±0.0250	0.172±0.0004	626±1.5650
10.35±0.3110	9.68±0.0240	0.170±0.004	640±1.6000

Table 1-Experimental Data

Preprints (www.preprints.org) | NOT PEER-REVIEWED | Posted: 11 October 2019 doi:10.20944/preprints201910.0133.v1

U_0 (m/s)	Power Output(W)	Torque (Nm)	RPM	ω(rads/s)	U_1	U_2	λ	Rotational Power(W)
4.22±0.1300	0.60±0.0020	0.046±0.0001	105±0.2620	11.00±0.0270	1.80±0.0540	0.50±0.0100	0.23±0.0290	0.51±0.0020
7.65±0.2300	1.42±0.0040	0.052±0.0001	270±0.6750	28.27±0.0730	1.92±0.0580	0.67±0.0130	0.33±0.0660	1.47±0.0770
9.39±0.2820	8.63±0.0220	0.161±0.0004	578±1.4500	60.53±0.1510	3.57±0.1070	1.64±0.0330	0.57±0.1590	9.72±0.0490
9.65±0.2890	9.94±0.0250	0.172±0.0004	626±1.5650	65.55±0.1640	3.74±0.1200	1.71±0.0340	0.60±0.1720	11.27±0.0540
10.35±0.3110	9.68±0.0240	0.170±0.0004	640±1.6000	67.02±0.1680	3.58±0.1070	1.62±0.0320	0.58±0.1790	11.39±0.0550

Table 2- Calculated Angular speed, Rotational Power and Tip speed ratio

U_0(m/s)	λ	Torque (Nm)	P_{actual}(W)	P_{aero} (W)	$C_{p,actual}$	$C_{p,aero}$(%)
4.22±0.1300	0.23±0.0540	0.046±0.0001	0.56±0.0020	1.45±0.1244	0.162±0.0150	0.420±0.0938
7.65±0.2300	0.33±0.0580	0.052±0.0001	1.45±0.0055	5.12±0.3860	0.071±0.0064	0.249±0131
9.39±0.2820	0.57±0.1070	0.161±0.0004	9.17±0.0355	14.02±1.6900	0.241±0.0210	0.369±0.0200
9.65±0.2890	0.60±0.1720	0.172±0.0004	10.60±0.0395	15.50±1.9400	0.257±0.0231	0.375±0.0203
10.35±0.3110	0.58±0.1790	0.170±0.0004	10.53±0.0395	17.19±2.0527	0.207±0.0187	0.338±0.0186

Table 3- Calculated, Actual Power, Aerodynamic Power and corresponding power coefficients

Preprints (www.preprints.org) | NOT PEER-REVIEWED | Posted: 11 October 2019 doi:10.20944/preprints201910.0133.v1

U_0 (m/s)	*a*	*m*
4.22±0.1300	0.573±0.0540	1.54±0.0640
7.65±0.2300	0.749±0.0580	1.22±0.0710
9.39±0.2820	0.620±0.1070	1.33±0.1410
9.65±0.2890	0.612±0.1120	1.34±0.1460
10.35±0.3110	0.654±.01070	1.29±0.1390

Table 4- Estimates of Induction Factor

$$U_1 = U_0(1-\bar{a}), \tag{21}$$

$$U_2 = U_0(1-(1.34\pm 0.1122)\bar{a}), \tag{22}$$

The plot of the difference in the pressure between the AVAWT inlet and outlet as a function of freestream speed is shown in Fig.3. The rhombic points are data points calculated from experimental measurements while the best fit for the data is the quadratic curve generated using the MATLAB curve fitting tool. A coefficient of determination of 86.1% is determined for this fit, resulting in a correlation coefficient of 92.8%. The coefficients of Eqns. (23) through (32) have been estimated within a 95% confidence interval (CI). Equation (23) below is the expression for the difference in pressure as a function of free stream speed;

$$P_2 - P_1 = 0.2147U_0^2 - 2.33U_0 + 7.269\ , \tag{23}$$

It is discernible from the curve that, the difference in pressure across the AVAWT increases parabolically with increasing freestream speed.

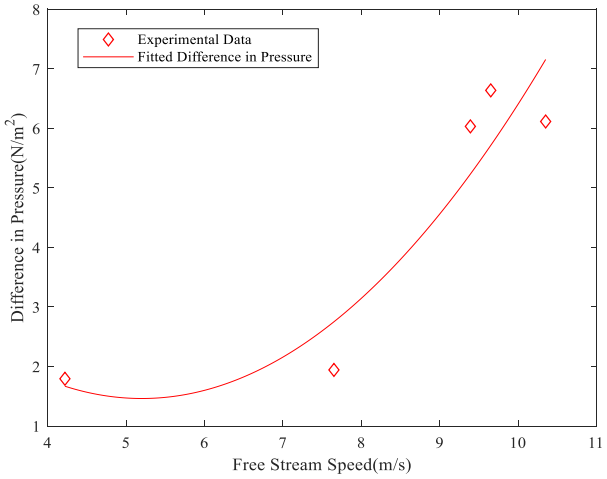

Figure 3- Difference in Pressure as a function of freestream speed

Figure 4 below depicts the plot of measured torque as a function of freestream speed. The square points are experimental data points while the best fit curve has been generated using the MATLAB curve fitting tool. It is seen from the curve that, the torque of the AVAWT increases exponentially with increasing freestream speed. A coefficient of determination of 86.14 is determined for this fit, resulting in a correlation coefficient of 92.81%. Equation (24) below is the expression for the torque as a function of freestream;

$$T(U_0) = 0.008922e^{0.2943U_0}, \tag{24}$$

Preprints (www.preprints.org) | NOT PEER-REVIEWED | Posted: 11 October 2019 doi:10.20944/preprints201910.0133.v1

The plot of measured torque as a function of tip speed ratio is depicted by Fig. 5. The square points are experimental data points while the best fit curve has been generated using the MATLAB curve fitting tool. A coefficient of determination of 99.48% was determined for the fit, resulting in a 99.90% correlation coefficient. The curve shows that there is a quadratic relationship between the tip speed ratio and the torque developed by the AVAWT model rotor. Equation (25) below is the expression for the torque as a function of tip speed ratio;

$$T(\lambda) = 0.9861\lambda^2 + 0.4562\lambda + 0.09753 \ , \tag{25}$$

$$P_{actual}(U_0) = 0.118e^{0.477U_0} - 1.209\times10^{11}e^{-6.408U_0} \ , \tag{26}$$

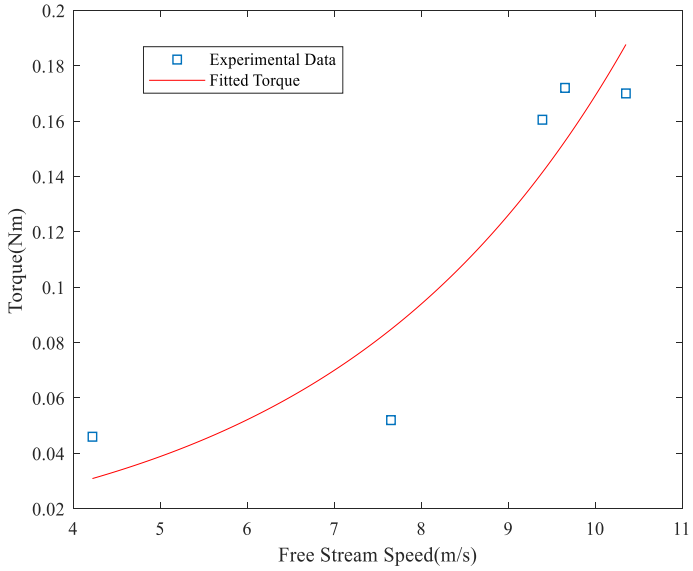

Figure 4- Plot of Torque as a Function of Free Stream Speed.

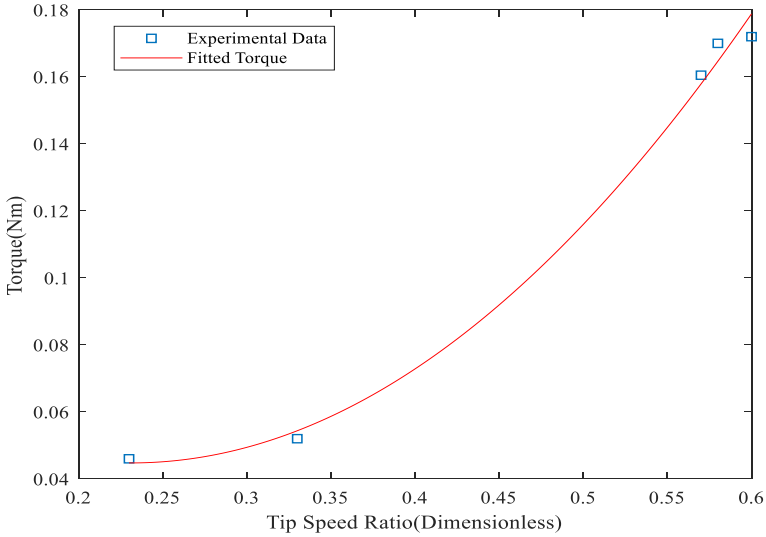

Figure 5- Plot of Torque as a Function of Tip Speed Ratio

The plot of measured power output as a function of freestream speed is shown in Fig. 6. The asterisks are experimental data points while the best fit curve has been generated using the MATLAB curve fitting tool. The fitted actual power curve is an exponential curve whose equation is Eqn. (26). It is discernible from the plot that,

Preprints (www.preprints.org) | NOT PEER-REVIEWED | Posted: 11 October 2019 doi:10.20944/preprints201910.0133.v1

the actual power generated by the AVAWT increases exponentially with increasing free stream speed. A coefficient of determination of 88.21% was determined for this fit, resulting in a correlation coefficient of 93.92%. Also shown in Fig.6 is the plot of the calculated aerodynamic power as a function of freestream speed. The square points are the data calculated from experimental measurements while the best fit curve has been obtained using the MATLAB plotting tool. There is a quadratic relationship between the aerodynamic power and the freestream speed. The equation relating the freestream speed to the aerodynamic power is Equation (27).

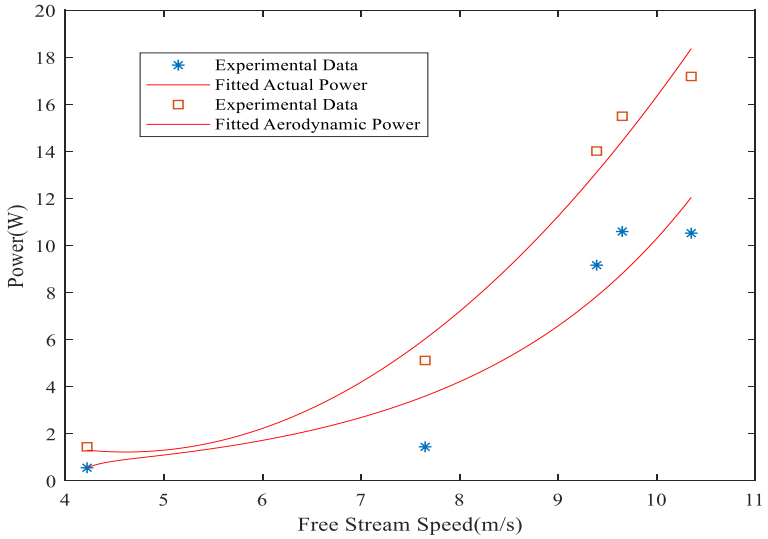

Figure 6-Plot of Power Output as a Function of Free Steam Speed

A coefficient of determination of 97.83 was determined for this fit, resulting in a 99.91% correlation coefficient. It is discernible from Fig.6 that, the aerodynamic curve follows the same trend as the measured power curve, but for the fact that, the aerodynamic power values are higher than the latter. The aerodynamic power increases from 1.45±0.1244W at 4.22±-.1300m/s to a maximum of about 18.4 W at 10.35±0.3110m/s while the actual power rises from0.56±0.1244W to about 12.1W within the same freestream speed range. It is also discernible from Fig. 6 that for freestream speeds between about 4.6m/s and 5.4m/s the aerodynamic power curve and the actual power curve nearly merge. This propensity for the curve to merge is the result of the fact that the power values are nearly equal within this range of freestream speed.

$$P_{aero}(\lambda) = 0.8579e^{4.961\lambda} \quad , \tag{29}$$

In Fig.7 below, the plots of actual power generated and the aerodynamic power respectively as functions of the tip speed ratio are shown. The aerodynamic power curve runs above the actual power curve because the aerodynamic power is higher than the actual power generated at all tip speed ratios. This difference is evident because, of friction on the bearings of the torque transducer and loss of power due to the conversion from kinetic energy to resistance heating in the windings of the torque transducer. Both curves rise from minima at a tip speed ratio of 0.23±0.0290 with the aerodynamic power at this point being about 2.5W while the actual power is 0.56±0.0020W; to maxima at a tip speed ratio of about 0.6±0.1720.

Preprints (www.preprints.org) | NOT PEER-REVIEWED | Posted: 11 October 2019 doi:10.20944/preprints201910.0133.v1

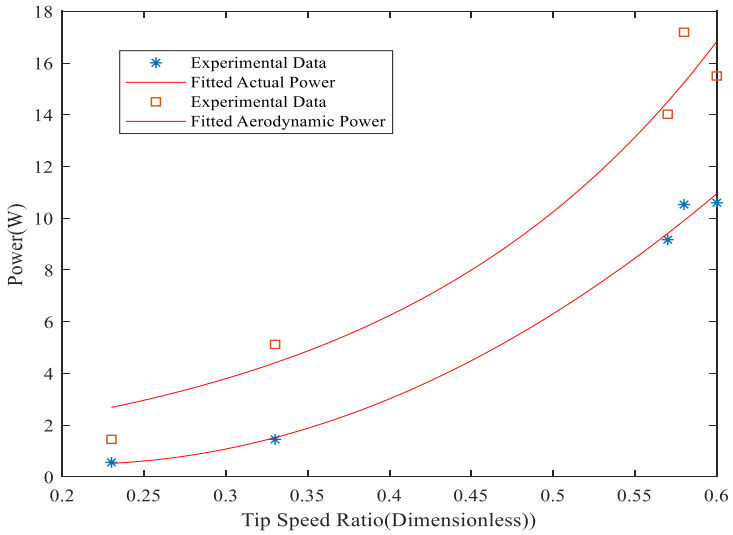

Figure 7- Plot of Power Output as a function of Tip speed ratio

At a tip speed ratio of 0.6±0.1720, the actual power read from the graph is about 10.9W while the aerodynamic power is about16.8W. The best fit for the actual power as a function of tip speed ratio determined with the MATLAB plotting tool is a quadratic polynomial as expressed in Eqn. (28). A coefficient of determination of 99.44% was determined for this fit, resulting in a correlation coefficient of 99.71%. An exponential curve is the best fit for plot of aerodynamic power as a function of tip speed ratio, λ. The relationship between the tip speed ratio and the aerodynamic power is expressed in Eqn. (29). A coefficient of determination of 95.94% was determined for this fit using the MATLAB plotting tool, resulting in a correlation coefficient of 97.95%. It is discernible from the plot that the aerodynamic power values are higher than the actual power generated. This difference in power is the result of the fact that, the aerodynamic power is derived from the rate of loss of kinetic energy by the airstream; something which does not account for the friction losses on the torque transducer bearings.

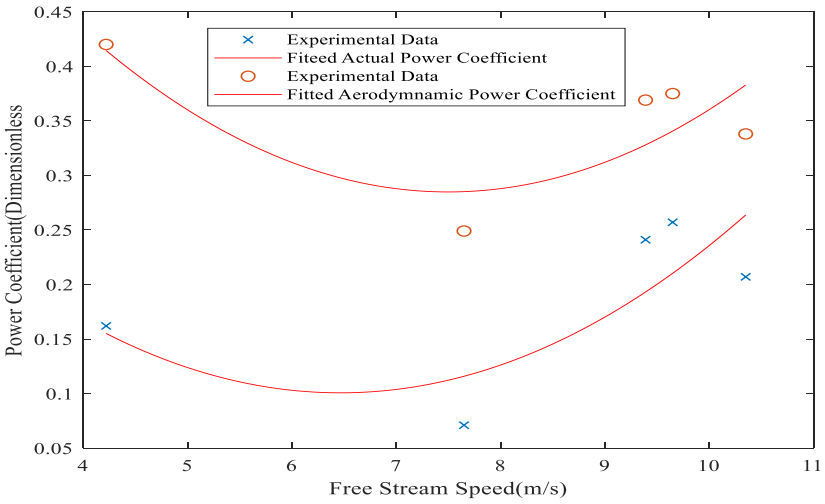

Figure 8- Power Coefficient as a Function of Freestream speed

Preprints (www.preprints.org) | NOT PEER-REVIEWED | Posted: 11 October 2019 doi:10.20944/preprints201910.0133.v1

Figure 8 depicts the plot of power coefficient as a function of free stream speed. The curve of actual power coefficient is below the curve of the aerodynamic power coefficient. There is a scatter between the experimental data and the fitted curve of actual power coefficient; same is true for the aerodynamic power coefficient. Both curves are parabolas with upward concavity, thus implying that both the aerodynamic and actual power coefficients vary quadratically with varying freestream speed. The curve of the actual power coefficient has a minimum value of about 0.1 at a freestream speed of about 6.5m/s while the curve of the aerodynamic power coefficient has a minimum value of about 0.28 at a freestream speed of about 7.3m/s. It is discernible from the graphs that, the aerodynamic power coefficient is higher than the actual power coefficient at all free stream speeds. This difference in power coefficient results from power losses due to drag, friction on bearings and losses in the generator windings. Equations (30) and (31) below express the relationship between the actual power coefficient, the aerodynamic power coefficient respectively and the free stream speed. A coefficient of determination of 56.25% was determined for Eqn. (30), using the MATLAB plotting tool; resulting in a correlation coefficient of 75. The coefficient of determination determined for Eqn. (31) is 61.73%, yielding a correlation coefficient of 78.57%.

$$C_{p,actual}(U_0) = 0.0198U_0^{\,2} - 0.1396U_0 + 0.552 \ , \tag{30}$$

$$C_{p,aero}(U_0) = 0.01206U_0^{\,2} - 0.1808U_0 + 0.9629 , \tag{31}$$

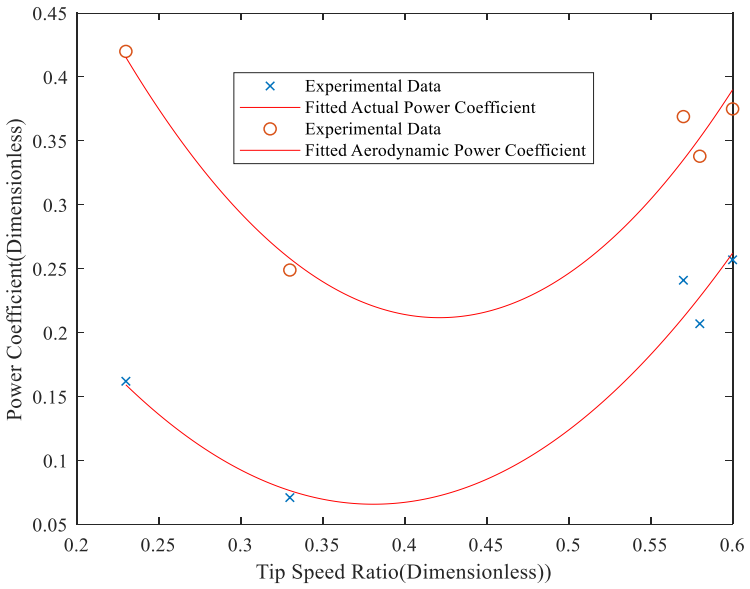

Figure 9- Plot of Power Coefficient as a Function of Tip Speed Ratio

Plots of respective Power coefficients as functions of the tip speed ratio are shown in Fig.9. It is discernible from the graphs that, the curve of the actual power coefficient has a minimum value of about 0.07 at a tip speed ratio of 0.38. The relationship between the actual power coefficient and the tip speed ratio is a quadratic polynomial as shown in Eqn. (32) below. A 93.99% coefficient of determination is determined using the MATLAB plotting tool for this fit, resulting in a correlation coefficient of 97.97%. The curve of the aerodynamic power coefficient has a minimum value of about 0.21 at a tip speed ratio of about 0.42. The relationship between the aerodynamic power coefficient and the tip speed ratio is also a quadratic polynomial

Preprints (www.preprints.org) | NOT PEER-REVIEWED | Posted: 11 October 2019 doi:10.20944/preprints201910.0133.v1

given by Eqn. (33). A coefficient of determination of 89.67% is determined using the MATLAB plotting tool for this fit, resulting in a correlation coefficient of 94.67%.

$$C_{p,actual}(\lambda) = 4.095\lambda^2 - 3.121\lambda + 0.6, \quad (32)$$

$$C_{p,aero}(\lambda) = 5.573\lambda^2 - 4.629\lambda, \quad (33)$$

It is discernible from Fig. 9 that, the aerodynamic power coefficient curve runs above the actual power coefficient curve. This is because, the aerodynamic power coefficient is higher than the actual power coefficient within the entire range of the tip speed ratios. The aerodynamic power coefficient is an indicator of the rate of change of kinetic energy as the air passes through the AVAWT while the actual power coefficient indicates the rate of energy conversion to electricity as the air flows past the AVAWT. It is worth noting that the best way to determine the power coefficient of a wind turbine (WT) is by measuring the actual power generated by the WT. The use of aerodynamic parameters to determine the power coefficient, results in higher values even when no power is generated.

Based on the results of the experiment, the average power coefficient due to the actual power generated by the AVAWT is 0.188±0.0168 while the average aerodynamic power coefficient of the AVAWT model rotor is about 0.350±0.0332, the power coefficient of a Savonius rotor is 0.30[3], the power coefficient of the Darrieus VAWT is between 0.4 and 0.42[4] and the power coefficient of a modified Savonius rotor with a 45° angle of twist is 0.3385[8]. It is worth noting that, unlike Darrieus type VAWTs that are not self-starting, the AVAWT is self-starting.

7.0 Wall Effects of the Wind Tunnel

Wind tunnel wall effects have an impact on the drag coefficient (C_D) and hence the drag on a model being tested in it. Damljanovic and others [21] discovered that for blockage ratios ranging from 0.5% to 0.6% and angles of attack within $\pm 10^{\circ}$, wind tunnel wall effects are negligible within measurement uncertainties. Other workers [22] performed numerical simulations on models with blockage ratios of 1.875% and 15% respectively and arrived at the conclusion that, the drag coefficient increased with increasing blockage ratio. Per these workers, it is reasonable to use the method of images in studying the wall effects of a wind tunnel on the drag experienced by a model being tested. In this study, the method of images is used to study the effects of the wind tunnel walls on the drag on the AVAWT model.

Awbi et al [23] working with a spherical model, discovered that, the drag coefficient did not vary with Reynolds number (Re) for Re ranging from 6.5×10^4 to 2.2×10^5, but it increased with increasing blockage ratio. This increase in drag coefficient is lower for critical values of Re than for less than critical Re. The increase in drag coefficient is lower for critical Re because the wake is narrower, resulting in a lower wake blockage effect. The method of images for blockage correction, splits wind tunnel wall effects into solid blockage (δ_s) due to the physical dimensions of the model and wake blockage (δ_w) due to the wake. Summing the two blockage factors yields the overall blockage factor (δ), where;

$$\delta = \delta_s + \delta_w, \quad (34)$$

The net effect of the wind tunnel wall is the sum of the induced speed and the wind tunnel free stream speed as expressed in eqn. (35) below [23]:

Preprints (www.preprints.org) | NOT PEER-REVIEWED | Posted: 11 October 2019 doi:10.20944/preprints201910.0133.v1

$$U = U_0(1+\delta), \quad (35)$$

For the AVAWT model, the effect of blockage is to reduce the wind tunnel velocity, since the rotor rotates with energy extracted from the air that flows past it. Thus, eqn. (35) becomes;

$$U = U_0(1-\delta), \quad (36)$$

After some algebraic manipulations on A. Thom's formula [23], the drag coefficient is given in terms of δ_w and the blockage ratio, r_b, as follows:

$$C_D = \frac{4\delta_w}{r_b}, \quad (37)$$

Implementing the results of this experiment, based on average conditions as determined in the foregoing sections Eqn. (36) can be expressed as;

$$1-\delta = 1-(1.34 \pm 0.1122)\delta_s, \quad (39a)$$

$$\delta = (1.34 \pm 0.1122)\delta_s, \quad (39b)$$

The blockage ratio r_b for the AVAWT model is 0.22 or 22% and from Eqns. (34) and (39b), $\delta_w = (0.34 \pm 0.1122)\delta_s$. Substituting these parameters in Eqn. (37a), yields;

$$C_D = 6.182\delta_s, \quad (40)$$

$$\delta_s = 1-(\frac{U_1}{U_0}), \quad (41)$$

Equation 40 and the expression for *Re* are coded in MATLAB and the resulting plot is shown in fig. 10 below.

Preprints (www.preprints.org) | NOT PEER-REVIEWED | Posted: 11 October 2019 doi:10.20944/preprints201910.0133.v1

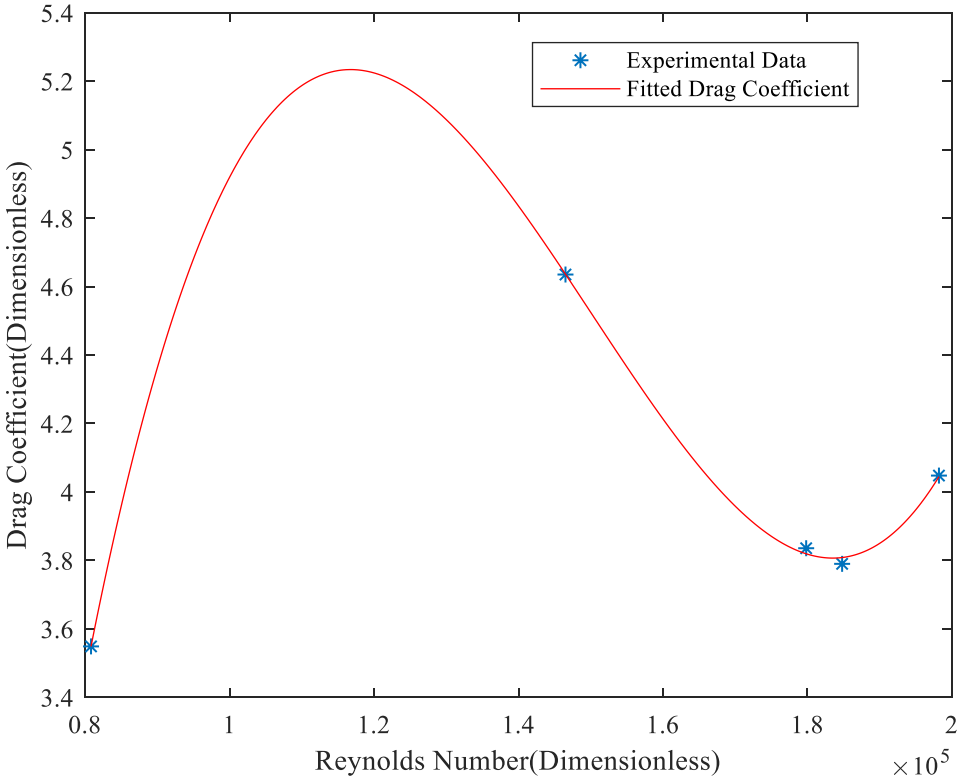

Figure10- Plot of Drag Coefficient as a Function of Reynolds Number

$$C_D = 9.591\times10^{-15}\,\mathrm{Re}^3 - 4.32\times10^{-9}\,\mathrm{Re}^2 + 6.164\times10^{-4}\,\mathrm{Re} - 23.12\,, \qquad (42)$$

The plot of drag coefficient as a function of Reynolds number, Fig. 10, is a cubic polynomial with a 99.91% coefficient of determination and a correlation coefficient of 99.95%. The relationship between the drag coefficient and the Reynolds number is given in Equation (42). It is discernible from the plot that, the drag coefficient increases from a value of about 3.55 at Re=8.1x10^4 to a peak of about 5.23 at Re ≅ 1.16x10^5 after which it drops to a trough of about 5.1 at Re ≅ 1.81x10^5. It then increases to a value of about 5.5 at Re≅ 1.96x10^5. The increase in the drag coefficient at Reynolds numbers between 8.1x10^4 and 1.16x10^5 may be the result of the thickening of the laminar boundary layer(LBL) near the walls of the wind tunnel; a phenomenon which results in an increase in the skin friction between the tunnel walls and the air; while the decrease in drag coefficient at Reynolds numbers between 1.16x10^5 and 1.81x10^5 may be the upshot of the thinning of the LBL. This thinning of the LBL results in a reduction in the skin friction between the tunnel walls and the air. The slight increase after the trough may be the result of random bombardment of the air particles, resulting in a narrowing of the wake of the AVAWT as the Reynolds number increases. This random motion of air particles is typical of turbulent flows. Since the drag on a model is directly proportional to its drag coefficient, the effects of wind tunnel walls on a model is to increase its drag. Thus, the wind tunnel walls increased the drag on the AVAWT rotor model and decreased its power output.

8.0 Conclusion

Within the limits of experimental errors, the average power coefficient of the AVAWT model based on the actual and aerodynamic power captured is 0.269±0.0250. Hence, the AVAWT model is less efficient than any of the afore-mentioned VAWTs. It is clear from this experiment that, the AVAWT can generate electricity if it

is coupled with a generator. While it is difficult to make a good comparison between the AVAWT model used in this experiment to existing VAWTs because, of the fact that, the AVAWT model is many times smaller than existing VAWTs-something which rendered it incapable of generating enough torque; a better power coefficient can be achieved using a larger size AVAWT and an open jet technique instead of testing in a wind tunnel. The walls of the wind tunnel test section also increased the drag on the AVAWT, which subsequently reduced its power output. A reduction in the drag on the AVAWT, could be achieved by using suitable airfoil blades with rectangular slots at the trailing edges instead of the rolled sheet metal blades currently used. The slot at the trailing edge of each airfoil blade will facilitate the flow of air through the blade from the positive pressure side to the low-pressure side, thus, reducing the drag and increasing the lift on the blade. This phenomenon which enhances flow from the high-pressure side to the low-pressure side through a slot at the trailing edge of an airfoil is known as boundary layer suction.

Much work remains to be done in studying the performance characteristics of the AVAWT. This includes numerical simulations and the quantification of the drag on the AVAWT using the wake speed distribution at selected free stream speeds.

Funding: This research received no external funding.

Acknowledgments: The permission to use his prototype rotor in the experiment, the construction of supports for instruments, the construction of the wind tunnel and the participation in the setup of the experiment by Bruce E. Anderson of No Fossil Fuel LLC; 348 Baldwin Road, Odenton, Maryland is highly appreciated.

Conflicts of Interest: The authors declare no conflict of interest.

References

1. Zayas, J; 2011," Scope of Wind Energy Generation Technologies", Energy and Power Generation Handbook by Rao K., R., ASME Press, Chap. 7. ISBN; 978-0-7918-5955-1
2. Manwell, J., F; McGowan, J, G; Rogers, A, L; 2011," Wind Energy Explained (Theory, Design and Applications)", 2e, Wiley, Chaps. 1-3. ISBN:978-0-470-01500-1
3. Taylor, D; 2012," Wind Energy"; Renewable Energy (Power for a Sustainable Future) 3e, by Boyle G., Oxford Press, Chap.7. ISBN:978-0-19-954533-9
4. D'Ambrosio, M; Medaglia, M; 2010," Vertical Axis Wind Turbines: History, Technology and Applications", Master's Degree Thesis in Energy Engineering; Hogskolan Halmstadt
5. Wekesa, D; Wang, C; Wei, Y; Kamao, J; Damao, L; 2014" A Numerical Analysis of Unsteady Inflow Wind for Site Specific Vertical Axis Wind Turbine: A Case Study for Marsabit and Garissa in Kenya", Renewable Energy, vol 76, Elsevier Ltd, pp 648-662.
6. Wekesa, D; Wang, C; Wei, Y; Damao, L; 2014," Influence of Operating Conditions on Unsteady Wind performance of Vertical Axis Wind Turbines Operating within a Fluctuating Free Stream: A Numerical Study", Journ. Engng. Ind. Aerodyn; vol135, Elsevier Ltd, pp76-89
7. Scheirich, F; Fletcher, T, M; Brown, R, E; 2010" Simulating the Aerodynamic Performance and Wake Dynamics of a Vertical Axis Wind Turbine," vol.14, Wind Energ., John Wiley, pp159-177,
8. Khan, J; Rhaman, M; 2014" Stress Analysis of Various Shaped Blade of Savonius Wind Turbine," ASME Paper No. IMECE2014-36307
9. Xisto C, M.; Pascoa J, C; Leger J, A; Transconi, M; 2014" Wind Energy Production Using an Optimized Variable Pitch Vertical Axis Rotor. ASME Paper No. IMECE2014-38966
10. Mucke, T; Kleinhans, D; Peinke, J; 2010, "Atmospheric Turbulence and its Influence on the Alternating Loads on Wind Turbines," vol. 14, Wind Energ, Wiley, pp301-316

11. McPhee, D; Beyene, A; 2016, "The Straight-Bladed Morphing Vertical Axis Wind Turbine," ASME Paper No. Power2016-59192
12. McLaren, K; Tullis, S; Ziada, S; 2011," Computational Fluid Dynamics of the Aerodynamics of a High Solidity, Small Scale Vertical Axis Wind Turbine," vol. 15, Wind Energ, Wiley, pp349-361
13. Scheurich, F; Brown, R., E; 2012," Modelling the Aerodynamics of Vertical Axis Wind Turbines in Unsteady Wind Conditions", vol.16, Wind Energ., Wiley, pp91-107
14. Zanon, A; Giannattasio , P; Ferreirra, C., J., S; 2012, " A Votex Panel Model for the Simulation of the Wake Flow Past a Vertical Axis Wind Turbine in Dynamic Stall", vol.16, Wind Energ2013, Wiley, pp661-680
15. Jaohindy, P; Ennamiri, H; Garde, F; Bastide, A; 2013, "Numerical Investigation of Airflow Through a Savonius Rotor,' Vol 17, Wind Energ.2014, Wiley, PP853-869
16. Edwards, J; M., Danao, L; A., Howell, R., J; 2013, "PIV Measurements and CFD Simulation of the performance and Flow Physics and a Small-Scale Vertical Axis Wind Turbine"' vol 18, WIND Energ2015, Wiley, pp201-217
17. Ragni, D; Ferreira, C., S; Correali, G., 2014," Experimental Investigation of an Optimized Airfoil for Vertical Axis Wind Turbines," vol.18, Wind Energ., Wiley, pp1629-1643,
18. Kundu, P; K; Cohen, I., M; 2004, "Fluid Mechanics", 3e, Elsevier Academic Press, Chap.4. ISBN:978-0-12-178253-5
19. Aris, R.; 1989, "Vectors, Tensors and the Basic Equations of Fluid Mechanics" Dover edition, Chaps. 4 through 6. ISBN: 0-486-66110-5.
20. Graebel, W; P., 2007, "Advanced Fluid Mechanics", Elsevier Academic Press, Chaps. 1 to 3. ISBN:978-0-12-370885-4.
21. Damljanovia, D; Vukovic, D; Ocokoljic, G; Rasuo, B; 2016, "A Study of Wall interference effects in Wind Tunnel Testing of a Standard Model at Transonic speeds", Proc. ICAS 2016.
22. Mokhtar, W; Hasan, M., R; 2016, "A CFD Study of Wind Tunnel Wall Interference", Proc. ASEE, N. Central Section Conference.
23. Awbi, H, B; Tan, S, H; 1983, "Effects of Wind-Tunnel Walls on the Drag of a Sphere", ASME Journ. Of Fluids Engineering,**103,** pp. 461-465. DOI: 10.1115/ 1.3240816.